ORIGINAL ARTICLE

ETRI Journal WILEY

Energy-efficient full-duplex UAV relaying networks: Trajectory design for channel-model-free scenarios

Nan Qi[1] [ID] | Wei Wang[1] | Diliao Ye[2] | Mei Wang[1] | Theodoros A. Tsiftsis[3] |
Rugui Yao[4] [ID]

[1]The Key Laboratory of Dynamic Cognitive Systems of Electromagnetic Spectrum Space, Ministry of Industry and Information Technology, Nanjing University of Aeronautics and Astronautics, Nanjing, China

[2]Telefonaktiebolaget LM Ericsson, Stockholm, Sweden

[3]The Institute of Physical Internet, Intelligent Systems Science, and Engineering, Jinan University (Zhuhai Campus), Zhuhai, China

[4]School of Electronics and Information, Northwestern Polytechnical University, Xi'an, China

Correspondence
Rugui Yao, School of Electronics and Information, Northwestern Polytechnical University, Xi'an, China.
Email: yaorg@nwpu.edu.cn

In this paper, we propose an energy-efficient unmanned aerial vehicle (UAV) relaying network. In this network, the channels between UAVs and ground transceivers are model-free. A UAV acting as a flying relay explores better channels to assist in efficient data delivery between two ground nodes. The full-duplex relaying mode is applied for potential energy efficiency (EE) improvements. With the genetic algorithm, we manage to optimize the UAV trajectory for any arbitrary radio map scenario. Numerical results demonstrate that compared to other schemes (eg, fixed trajectory/speed policies), the proposed algorithm performs better in terms of EE. Additionally, the impact of self-interference on average EE is also investigated.

KEYWORDS
Energy efficiency, full-duplex relaying, genetic algorithm, model-free channel gain, unmanned aerial vehicle

1 | INTRODUCTION

As an emerging technology, unmanned aerial vehicles (UAVs) are being developed for various applications, including UAV-assisted smart city architectures, agriculture, and industrial development [1]. In particular, UAV-integrated communications have attracted significant research attention [1,2] (and

the references therein), particularly for urgent or dangerous communication scenarios (eg, border detection and remote sensing). Such applications are facilitated by the low cost, deployment flexibility, and full controllability in 3D airspaces of UAVs. Compared to terrestrial systems, UAV wireless systems offer several advantages, including superior link quality for communication channels [3] and greater link connection

flexibility [4]. Therefore, UAV-enabled communications are expected to improve network capacity and increase cell coverage in emerging 5G networks [5]. In particular, UAV relaying techniques have seen many applications for assisting in communication between two distant nodes [6–9]. Numerous investigations have been conducted both experimentally and theoretically. Experimentally, some UAV projects have captured videos over specified areas [8]. Theoretically, it has been verified that compared to direct base station (BS)-ground user transmissions, UAV relaying systems with appropriate UAV positioning can approximately double end-to-end capacity. The authors of [9] investigated the throughput maximization problem for half-duplex UAV relaying networks by jointly optimizing transmission power and UAV trajectories. It has been demonstrated that significant throughput gains can be achieved compared to the conventional static relaying mode.

Although UAV relaying techniques introduce many new opportunities, they also come with several shortcomings. In practice, a UAV has a finite flying duration determined by its practical weight and onboard battery capacity. Small- and medium-sized UAVs on the market today generally have a battery capacity of 2300 to 5400 mAh and maximum flight duration of 5 to 30 minutes [10–12]. Therefore, energy efficiency (EE), which is measured as the number of successfully transmitted bits per unit energy, has become a key performance indicator. In [13–15] energy-efficient terrestrial half-duplex relaying (HDR) transmissions were investigated and transmission power was optimized. The EE maximization problem for slotted transmissions was investigated in [15]. The authors of [16] and [17] focused on UAV trajectory design to maximize EE by considering the energy consumption of UAV propulsion systems. However, previous works have largely considered direct transmission scenarios. To improve the EE of UAV relaying networks, in addition to power management, two other aspects have been considered in [2,6,9,14,15,18] and [19]. One method is to optimize UAV flight mobility characteristics, including flight paths and speeds [2,9,14,18,20,21]. This method is motivated by the fact that UAV flight behaviors are closely related to channel conditions. In particular, flight propulsion consumption accounts for a large proportion of overall energy consumption. The second method is to reduce data transmission durations by applying efficient communication techniques, such as full-duplex (FD) mode, [20] where data receiving and transmitting are performed simultaneously. When the data transmission time is reduced, the duration of UAV task execution can also be reduced, providing a chance to reduce flight energy consumption.

For UAV-assisted communication systems, two types of channels are used: air-to-ground (ATG) and ground-to-air (GTA) channels. ATG and GTA propagations are more complicated in urban environments than in rural areas. Consider an ATG channel as an example, radio signals propagate through free space until they reach an urban environment, where shadowing and scattering are caused by complex terrain structures. The authors of [21–23] established a simplified probabilistic mean path loss model using the averages of line-of-sight (LoS) or non-LoS channel gains [21,23]. In [21] and [22], the probability of having an LoS connection between a ground user and UAV was characterized based on the elevation angle between the user and UAV. In [23], channel gain was modeled based on the statistical parameters of underlying urban environments, including the statistical distribution of building heights and number of buildings per unit area. However, these studies were performed based on coarse-grained terrain structures and failed to exploit fine-grained propagation conditions. Fined-grained channel conditions are difficult to characterize mathematically based on a few factors. First, channel gains consist of multiple attenuations, including large-scale path loss and shadowing, as well as small-scale fading caused by multipath propagations. In urban areas, channel gains may have a complex structure based on the irregular shapes of terrain. Second, additional random interferences are induced by other devices that communicate at the same frequency.

Although UAV trajectory optimization problems have been extensively investigated in delay-tolerant networks [2,6,9,14,18–21], previous studies have mainly focused on specific channel models or statistical distributions. For channel-model-free scenarios, it is impossible to derive exact channel model expressions. Therefore, traditional model-driven algorithms such as the convex-based algorithm [14] and rapidly exploring random trees algorithm [24] are not applicable. Alternatively, as evolutionary algorithms, genetic algorithms (GAs) provide heuristic search methods. A GA is essentially an iteration-based optimization technique that learns from past iterations and evolves over time. Although they are simple in design, GAs have been demonstrated to be efficient for solving a series of complex and non-deterministic problems. Therefore, GAs have attracted significant research attention and have been applied in various engineering fields (eg, function optimization [25], automatic control [26], and image manipulation [27]).

In particular, GAs have been extensively studied in wireless communication resource management problems [28], where their advantages in terms of finding close-to-optimal solutions for various optimization problems with low complexity are particularly useful [29] (and the references therein). The authors of [30] studied UAV-assisted caching networks using GAs. Numerical results demonstrated that compared to traditional strategies, GAs can better solve the probabilistic caching placement problem by maximizing the average service success probability in heterogeneous wireless networks. The authors of [28] optimized the location of an FD relay node to minimize outage probabilities for faraway users in a cognitive system. In [28] and [31], relay problems with discrete and continuous variables were investigated. In [31], a two-hop HDR multi-session routing scheme was studied, where a moving relaying vehicle was deployed to deliver data for isolated communities formed following disasters. The relay scheduling problem can be formulated as an integer programming problem and solved efficiently using

a GA. In [28], the authors investigated how to minimize deployment costs and improve quality of service performance. A GA was also applied to find discrete solutions. Similar to [31], the authors of [32] designed a data-ferry-UAV traveling policy for disaster-affected areas. Specifically, BSs rely on a flyby UAV to collect, carry, and transmit data periodically to a core network. A UAV visiting sequence that minimized the overall energy consumption for data delivery was also designed. The authors of [33] investigated the age-optimal trajectory planning problem in UAV-enabled data collection networks. In this problem, a UAV flies at a constant flight velocity while collecting data from ground nodes. The UAV visiting sequence is optimized using a GA and dynamic programming method.

Related works in [31,33,34], and [35] considered a dedicated message ferry network. However, the data transmission quality and UAV energy costs were not considered. EE performance was ignored, and a potential energy-efficient full-duplex relaying (FDR) scheme was not exploited. Additionally, the data transmission rate is closely related to the UAV position because channel quality is affected by the UAV position. However, this aspect was not considered in [31,35]. Although the authors of [32] combined trajectories with design metrics, they mainly focused on UAV visiting sequences, which are not applicable to relaying systems.

1.1 | Our contributions

Among UAV trajectory planning problems, we observed that energy-efficient FDR UAV trajectory planning in channel-model-free networks is still an open issue. In this study, we attempted to optimize FDR UAV trajectories without relying on channel model assumptions.

Specifically, our main contributions can be summarized as follows:

1. An FDR UAV relaying scheme is proposed for a channel-model-free scenario and an FDR UAV EE optimization problem is formulated.
2. We propose a GA to search intelligently for near-optimal UAV trajectories. The convergence behaviors of the GA are analyzed, revealing that the GA works well for the FDR UAV EE optimization problem.
3. The advantages of the proposed scheme over fixed-speed/trajectory policies and HDR models are demonstrated. Additionally, the impact of the self-interference (SI) cancelation factor is also analyzed. The results indicate that our scheme outperforms other FDR benchmark schemes and yields more than five-fold EE gains for scenarios with small SI cancelation factors.

The remainder of the paper is organized as follows. Section II details out system model. The FDR UAV EE optimization problem is formulated in Section III. Problem solving based on a GA is presented in Section IV. Numerical results are presented and analyzed in Section V. Section VI concludes this paper.

2 | SYSTEM MODEL

We consider a scenario in which a rotary-wing UAV is dispatched as a flying relay to communicate with multiple ground nodes sequentially. Therefore, multiple flight periods with various durations are considered [36]. Without loss of generality, we consider the flight period from one given takeoff point to one destination as an illustrative example. The reasons why a UAV has a final destination point are outlined below. (1) In practice, final UAV locations depend on UAV launching/landing locations and their pre- and post-mission flying paths [9]; (2) based on practical limitations in terms of size, weight, and onboard battery capacity, a UAV has a finite service duration [20]; (3) when in flying mode, a UAV has advantages compared to the hovering mode in terms of EE performance [36].

As shown in Figure 1, severe path loss or physical obstacles are present between S_1 and S_2. A rotary-wing UAV acts as a mobile relay to assist in message transmission. To exploit relaying capacity fully and enhance data transmission EE, an FDR scheme is designed for a UAV. The UAV is equipped with two antennas: one receiving and one transmitting antenna. The rotary-wing UAV flies within a specified aerial area for a predetermined duration to assist in relaying signal transmissions. One complete transmission consists of two phases: S_1-UAV first-hop transmission and the UAV-S_2 data forwarding phase. We provide detailed explanations of these phases in Sections 2.1 and 2.2, respectively. Additionally, we assume that the UAV has a global positioning system and can automatically follow a predetermined trajectory [37].

Let the time horizon T represent the flight period from S_1 to S_2. For mathematical tractability, we uniformly discretize T into M time intervals with durations of $\Delta_m = T/M$. Based
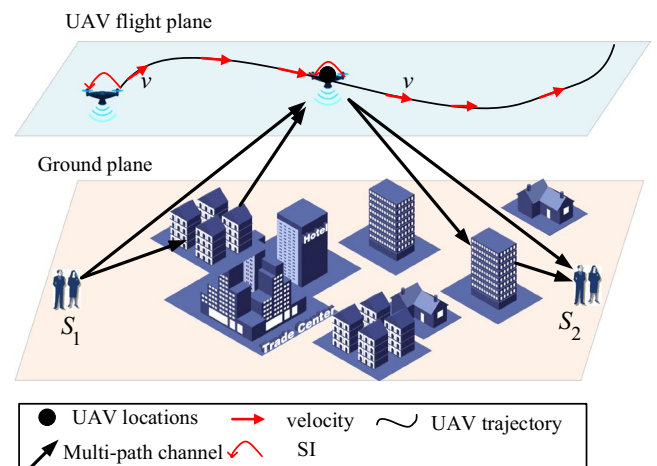

FIGURE 1 Full-duplex UAV-assisted relaying system

on the existence of processing delays, received signals cannot be immediately forwarded. Here, we set the processing delay to τ time intervals (ie, $\tau \cdot t_m$ s). For ease of analysis and without loss of generality, we let τ be an integer. The lengths of each segment, denoted as $DD_m(m = 1, 2, \ldots, M)$, are not necessarily identical and can vary the flying velocity in each segment.

In practical scenarios, channel power gain is a superposition of small and large fading phenomena, which are both considered in our model. It is a function of 3-tuple variables, including location X, frequency f, and time t. The channel power gain in the ith transmission phase is denoted as ($i = 1$ and 2 represent the first and second phases respectively, which will be illustrated in Sections 2.1 and 2.2, respectively).

$$g_i(x, f, t) = \frac{|\varsigma_i(X, f, t)|^2}{K[d_i(X, t)]^{-a_i(X, f, t)}}, \quad (1)$$

where $\varsigma_i(X, f, t)$ is the channel gain that combines various fading phenomena, excluding free-space path loss. $[d_i(X, f, t)]^{-ai(X, f, t)}$ represents the free-space path loss, $a_i(X, f, t)$ is the exponent, $d_i(X, t)$ is the communication distance, and $K = \frac{PL(d_0)}{d_0^a}$ is a constant used in the log-distance path loss model, where $PL(d_0)$ is the linear path loss at a reference distance d_0. Without loss of generality, K is normalized to unity. It should be noted that the set of $g_i(x, f, t)(\forall X, f, t)$ describes a radio map of an aerial area for a given spectrum and time horizon.

For ease of expression, in the following discussion, we consider one sample (ie, a given combination (X, f, m)) as an example to illustrate data transmission. Therefore, (1) can be reduced to

$$g_{i,m} = |\varsigma_i(x, y, m)|^2 d_{i,m}^{-a_{i,m}}, \quad (2)$$

where $|\varsigma_i(x, y, m)|^2$ is the channel power gain at point (x, y) in the mth time interval, and $d_{i,m}$ and $a_{i,m}$ are the line-of-sight communication distance and exponent in the mth time interval of the ith transmitting phase ($i = 1$ and 2).

2.1 | S_1-UAV data transmission

The signal received at a UAV can be formulated as

$$y_{r,m} = \underbrace{\sqrt{P_1 |\varsigma_1(x, y, m)|^2 d_{1,m}^{-a_{1,m}}} S_{t,m}}_{\text{Transmitted signal from } S_1}$$
$$+ \underbrace{\sqrt{P_r |h_{rr}|^2 k_0 S_{r,m}}}_{\text{UAV self - interference}} + n_1, \quad m = 1, 2, \ldots, M, \quad (3)$$

where the first term is the signal from S_1 at the beginning of the mth time interval, the second term is the SI, and P_1 and

P_r represent the data transmitting powers at S_1 and the UAV relay, respectively. k_0 and h_{rr} are the SI cancelation factor and small-channel fading of the UAV SI channels, respectively. n_1 is the additive white Gaussian noise (AWGN) at the UAV with a mean power of σ_1^2.

Because there is a processing delay at the UAV, received signals cannot be immediately forwarded. Here, we set the processing delay to τ time intervals (ie, $\tau \frac{T}{M}$ s). The decoding-and-forwarding relaying protocol is adopted. Specifically, when the UAV can successfully decode a received signal, the forwarded signal from the UAV to S_2 in the mth time interval is $S_{t, m-\tau}$ (ie, $S_{r,m} = S_{t, m-\tau}$).

The S_1-UAV signal-to-interference ratio in the mth time interval is calculated as.

$$SINR_{1,m} = \frac{P_1 |\varsigma_1(x, y, m)|^2 d_{1,m}^{-a_{1,m}}}{k_0 P_r |h_{rr}|^2 + \sigma_1^2}. \quad (4)$$

Then, the channel capacity is calculated as.

$$C_{1,m} = B\log_2(1 + SINR_{1,m}). \quad (5)$$

2.2 | UAV-S_2 signal forwarding

The signal received at S_2 is

$$y_{S_2} = \sqrt{P_r |\varsigma_2(x, y, m)|^2 d_{2,m}^{-a_{2,m}}} S_{t, m-\tau} + n_2, \quad m = 1, 2, \ldots, M, \quad (6)$$

where n_2 is the AWGN at S_2.

It can be derived that the SINR at S_2 in the mth time interval is.

$$SINR_{2,m} = \frac{P_r |\varsigma_2(x, y, m)|^2 d_{2,m}^{-a_{2,m}}}{\sigma_2^2}. \quad (7)$$

Based on the transmission delay of τ time intervals, we have $C_{2,m} = 0$ when $m = 1, 2, \ldots, \tau$. Therefore, the channel capacity of the UAV-S_2 link can be calculated as follows:

$$C_{2,m} = \begin{cases} 0, \text{ when } m = 1, 2, \ldots, \tau, \\ B\log_2(1 + SINR_{2,m}), \text{ otherwise.} \end{cases} \quad (8)$$

3 | EE OPTIMIZATION PROBLEM FORMULATION

We aim to maximize overall EE by optimizing UAV trajectories under the UAV mobility constraints. The objective function, denoted as η_{EE}, is defined as

$$\eta_{EE} = \frac{\sum_{m=\tau}^{M-1} R_m}{\sum_{m=\tau}^{M-1} P_{tot,m}}, \quad (9)$$

where R_m and $P_{tot,m}$ are the data transmission rate and overall power consumption in the m th time interval, respectively.

In the following subsections, the objective function and constraints are formulated in detail.

3.1 | Sum-capacity formulation

Let $C'_{1,m}\Delta_m$ represent the bit budget (upper bound of the number of transmitted bits in the mth time interval) of the UAV, including any bits accumulated prior to the mth time interval and the newly received bits in the mth time interval. The number of accumulated bits received prior to the mth time interval can be calculated as $\max\{(C'_{1,m-1}\Delta_{m-1} - C_{2,m-1}\Delta_{m-1}), 0\}$. Additionally, the number of newly received bits in the mth time interval is $C_{1,m}\Delta_m$. Then, we have the following recursive expressions:

$$C'_{1,1}\Delta_1 = C_{1,1}\Delta_1, \tag{10}$$

$$C'_{1,2}\Delta_2 = C_{1,2}\Delta_2 + C_{1,1}\Delta_1, \tag{11}$$

$$C'_{13}\Delta_3 = C_{1,3}\Delta_3 + \max\left\{\left(C'_{1,2}\Delta_2 - C_{2,2}\Delta_2\right), 0\right\}, \tag{12}$$

$$C'_{1,m}\Delta_m = C_{1,m}\Delta_m + \max\left\{\left(C'_{1,m-1}\Delta_{m-1} - C_{2,m-1}\Delta_{n-1}\right), 0\right\}, \tag{13}$$

where Δ_m is the duration of the m th time interval. Without loss of generality, we set $\Delta_1 = \Delta_2 = \ldots = \Delta_m = \Delta = T/M$.

Information causality requires that the number of transmitted bits in the mth time interval must be less than or equal to $C'_{1,m}\Delta_m$ (ie, $R_m\Delta_m \leq C'_{1,m}\Delta_m$). Additionally, the Shannon capacity theory requires that $R_m\Delta_m \leq C_{2,m}\Delta_m$, or equivalently, $R_m \leq C_{2,m}$. To optimize EE, R_m should be maximized as

$$R_m = \min\left\{C'_{1,m}, C_{2,m}\right\}. \tag{14}$$

This is because the number of bits can be increased to the maximum allowable value without decreasing the objective value or violating the information causality constraint. Therefore, R_m is driven to reach its upper bound (ie, $\min\left\{C'_{1,m}, C_{2,m}\right\}$).

In Sections 3.2 and 3.3, $P_{tot,m}$ and the aforementioned constraints, respectively, are introduced in detail.

3.2 | Overall power consumption formulation

Overall power consumption consists of UAV propulsion, SI cancelation, and communication consumption. We only focus on the first component here because it is much larger than the other two components, as discussed in [36]. The UAV power model presented in [36] was adopted in this study. The flight distance of the m th time interval is

$$DD_m = \sqrt{(x_m - x_{m-1})^2 + (y_m - y_{m-1})^2}, \tag{15}$$

where $D_{x,m} = x_m - x_{m-1}, D_{y,m} = y_m - y_{m-1}$, and $m = 1, 2, \ldots, M$. Additionally, the flying speed in the m th time interval is given as

$$v_m = \frac{DD_m}{T/M} = \sqrt{v_{x,m}^2 + v_{y,m}^2}, \tag{16}$$

where $v_{x,m}$ and $v_{y,m}$ are the speeds along the X and Y axes in the m th time interval, respectively. Additionally, we define $\boldsymbol{v}_x = \{v_{x,1}, v_{x,2}, \ldots, v_{x,M}\}$, and $\boldsymbol{v}_y = \{v_{y,1}, v_{y,2}, \ldots, v_{y,M}\}$.

Let P_0 and P_i represent the blade profile power and induced power, respectively, which can be formulated as [36]

$$P_0 = \frac{\varepsilon}{8}\rho s A\Omega^3 R_0^3, \quad P_i = (1 + k_h)\frac{W^{3/2}}{\sqrt{2\rho A}}, \tag{17}$$

where ε is the profile drag coefficient, ρ is the air density, s is the rotor radius, A is the rotor disk area, Ω is the blade angular velocity in radians, R_0 is the rotor radius (measured in meters), k_h is the incremental correction factor for the induced power, and W is the aircraft weight in Newtons.

The overall power consumption is calculated as

$$E_{tot} = \sum_{m=\tau}^{M}\left[P_0\left(1 + \frac{3DD_m^2}{U_{tip}^2 \cdot T^2/.M^2}\right) + \frac{P_i v_0}{DD_m}\frac{T}{M} + \frac{1}{2}\eta\rho s A\frac{DD_m^3}{T^3}M^3\right], \tag{18}$$

where U_{tip} and v_0 are the tip speed of the rotor and mean rotor induced velocity in the hovering state, respectively, and η is the fuselage drag ratio.

3.3 | Constraint formulation

3.3.1 | Constraints on the data transmission rate

As discussed in Section 3.1, (14) must be satisfied.

3.3.2 | Constraints on UAV mobility behavior

In practice, the UAV's starting and ending points are predetermined and depend on various factors such as the UAV's takeoff/landing locations, as well as its mission flying path. The initial location (x_0, y_0, H) and end location (x_M, y_M, H) must satisfy

$$x_0 = x_s, y_0 = y_s, x_M = x_Z, y_M = y_Z. \tag{19}$$

Additionally, the UAV flying speed is bounded by a maximum value of $V_{\max}$. It is required that

$$DD_m \le V_{\max}\frac{T}{M}, \quad \forall m, m = 1, 2, \ldots, M. \tag{20}$$

3.4 | Optimization problem

When V_x and V_y are given, a trajectory can be determined. In other words, optimizing the trajectory is equivalent to deriving the optimal velocity vector.

Our optimization problem aims to search for the optimal velocity vector such that EE can be maximized as

$$\mathbf{P1}: \max_{V_x,V_y} \eta_{EE} = \frac{\sum_{m=\tau}^{M} R_m}{\sum_{m=\tau}^{M} P_{tot,m}} \tag{21}$$

$$s.\,t. \quad [20],$$

$$x_s \le x_m \le x_z, \ y_s \le y_m \le y_z, m \in \{1, 2, \ldots, M\}. \tag{22}$$

4 | PROBLEM SOLVING USING A GA

4.1 | Objective function and constraint transformation

In the following analysis, a penalty method is applied to convert the constrained optimization problem into an unconstrained problem. In this section, we define two penalty functions that describe violations of constraints (20) and (22).

First, let f_1 denote the penalty for a trajectory policy if it violates (20). f_1 is defined by the Normalized value of $(v_m - V_{\max})$ if $|v_m| > V_{\max}$. This value indicates the extent to which the flying speed violates constraint (20). It should be noted that the expression of f_1 is not unique. In the following analysis, f_1 is defined as

$$f_1 = \max\left\{\frac{\tilde{v} - v_{\max}}{|\tilde{v}' - v_{\max}| + c_1}, 0\right\}, \tag{23}$$

where $\tilde{V}$ is the maximum flying speed among M intervals for one trajectory, meaning

$$\tilde{V} = \max\left\{\sqrt{v_{x,1}^2 + v_{y,1}^2}, \sqrt{v_{x,2}^2 + v_{y,2}^2}, \cdots, \sqrt{v_{x,M}^2 + v_{y,M}^2}\right\}. \tag{24}$$

Here, $\tilde{v}'$ is the maximum flying speed among all intervals in multiple trajectory policies and c_1 is introduced as a positive value so that the denominator in (23) is positive. It should be noted that $c_1 = |\tilde{v}' - v_{\max}|$ such that the impact of c_1 on f_1

can be ignored. Based on the above analysis, it can be concluded that $f_1 \in [0, 1)$.

For any trajectory policy, if it ends with a position other than the destination, a penalty is imposed on the policy. The distance offset is normalized. Specifically, we let $f_2 \in [0, 1]$ indicate the extent to which a trajectory violates constraint (22). $f_2 = 1$ represents the maximum distance offset among all populations. Specifically, f_2, is formulated as follows:

$$f_2 = \frac{\sqrt{(x_M - x_z)^2 + (y_M - y_z)^2}}{\tilde{D}_M + c_2}, \tag{25}$$

where $\tilde{D}_M$ is the maximum offset of (x_M, y_M) relative to (x_z, y_z) among the multiple trajectory policies in (22) and c_2 is introduced as a positive value so that the denominator in (25) is positive. It should be noted that $c_2 \ll \tilde{D}_M$ such that c_2 has a very limited impact on f_2.

Let c_4 and c_5 represent the penalty coefficients for f_1 and f_2, respectively. The weighted EE for a single trajectory, denoted as $\eta_{EE}^{(w)}$, is calculated as

$$\eta_{EE}^{(w)} = \eta_{EE} - (\eta_{\max} - \eta_{\min} + c_3) \cdot (c_4 f_1 + c_5 f_2), \tag{26}$$

where $\eta_{\max}$ and $\eta_{\min}$ are the maximum and minimum EE values, respectively, and c_3 is a small positive constant. Here, $\eta_{\max} - \eta_{\min} + c_3$ is introduced to guarantee that at least one policy will be finalized if constraints (20) and (22) are violated. Additionally, the expression of $\eta_{EE}^{(w)}$ is not unique and there may be numerous variations in (26).

In summary, the trajectory optimization problem **P1** can be converted into an unconstrained optimization problem **P2** as follows:

$$\mathbf{P2}: \max_{V_x,V_y} \eta_{EE}^{(w)}. \tag{27}$$

The optimal trajectory solution is denoted as.

$$I^* = \text{argmax}(\eta_{EE}^{(w)}). \tag{28}$$

The optimal solution must satisfy $\eta_{EE}^{(w)}(I^*) = \eta_{EE}(I^*)$. This is because in an optimal solution, the constraints must be satisfied, leading to zero penalties in terms of EE.

4.2 | GA design

In this section, a GA is applied to solve **P2**. The basic concept is to generate a population of candidate trajectory policies and let them evolve through crossover and mutation operations such that the trajectory policies converge toward better solutions and an optimal solution can be gradually approximated. We first provide detailed definitions of a chromosome, population, and the fitness function in problem **P2**.

Chromosome: The vector of flying velocity in the X and Y axes (ie, $\mathbb{C}^{1 \times 2M} = \left[v_{x,1}, v_{x,2}, \ldots, v_{x,M}, v_{y,1}, v_{y,2}, \ldots, v_{y,M}\right]$). The length of a chromosome is $2M$.

Population: The set of chromosomes. A population of size N_p is denoted as $\mathbb{P} N_P \times 2M = \left[\mathbb{C}_1, \mathbb{C}_2, \ldots, \mathbb{C}_{N_P}\right]^{\mathrm{T}}$, where $[\cdot]^{\mathrm{T}}$ is a transpose operator.

Fitness function: The value of the objective function (ie, $\eta_{\mathrm{EE}}^{(w)}$).

The evolution process involves coding, selection, recombination, and mutation. By merging chromosomes from parents and offspring, new chromosomes are generated and the population is updated. The steps listed above are then repeated until the number of generations reaches a predetermined number, after which the chromosome with the maximum fitness value is selecting as the final flying velocity vector. The details of this process are discussed below.

1. **Coding**: We use binary coding to map flying velocities into binary symbol sequences (ie, a string of 0s and 1s)
2. **Selection**: An elitist selection method is applied. This means that in each generation, the worst individual is removed from the population. The other chromosomes undergo recombination and mutation. The best chromosome with the largest fitness function value is recorded and retained in the next generation without any modification.
3. **Recombination**: We use a two-point intersection method to obtain new individuals via gene exchange. The probability of variation for each chromosome is denoted as Pr_c.
4. **Mutation**: After recombination, individuals undergo mutations. The probability of variation for each gene is denoted as Pr_v.

Algorithm 1 summarizes the process of the proposed trajectory optimization strategy.

Algorithm 1 Energy-efficient FDR UAV with a GA

Input:
Randomly generated initial chromosomes and population Q_0; Initial generation index: $N_g = 1; T, M, N_p, c_1, c_2, c_3, c_4, c_5, Pr_c, Pr_v$.

Output:
The best individual I^*;

1. **while** $= N_g \leq 300 \,\& \, | \frac{\eta_{\mathrm{EE}}(N_g) - \eta_{\mathrm{EE}}(N_g - 1)}{\eta_{\mathrm{EE}}(N_g)} | > 10^{-3}$ **do**
2. Obtain fitness values by computing $\eta_{\mathrm{EE}}^{(w)}$ in the N_g th generation (ie, $\eta_{\mathrm{EE}}^{(w)}(N_g)$);
3. Record the best individual $I_{N_g}^* = \mathrm{argmax}(\eta_{\mathrm{EE}}^{(w)}(N_g))$;
4. Select $(N_p - 1)$ individuals with high fitness values in the N_g th generation, the set of which is denoted as $Q_1(N_g)$;
5. Recombine individuals in $Q_1(N_g)$ and obtain a new individual set $Q_2(N_g + 1)$. The number of individuals in $Q_2(N_g + 1)$ is identical to that in $Q_1(N_g)$;
6. Mutate: Each individual in Prv, Prc;
7. The set of all new individuals is denoted as $Q_3(N_g + 1)$;
8. A new generation, denoted as $Q(N_g + 1)$, is formed by integrating $I_{N_g}^*$ into $Q_3(N_g + 1)$;
9. $N_g = N_g + 1$;
10. **end while**
11. $I^* = I_{N_g}^*$

---

5 | NUMERICAL RESULTS

In this section, we present analytical results. Additionally, EE under the FDR scheme is compared with that under the HDR scheme.

The parameter settings use the values listed in Table 1 unless otherwise specified. Without loss of generality, the UAV departure point is set to (0, 3000) and the intended destination is set to (1000, 3000). Additionally, for all of the analyzed schemes, the overall UAV flight duration is set to $T = 25$ s, which is discretized into $M = 25$ segments of equal length. The settings of the parameters in (17) and (18) are also adopted in the method from [36]. Detailed channel power gains for the target two-dimensional space are available online (please access [38] with the code "8pao"). Without loss of generality, we assume that $|\varsigma_1(x, y, m)|^2 = |\varsigma_2(x, y, m)|^2. \forall m$. In the file, [38] the value in the ith row and jth column represents the channel power gain at point (x_i, y_j) (measured in meters), while the channel power gains in other locations are approximated based on those of their closest neighboring nodes in the data file.

5.1 | Data illustrations

In Figure 2, the numbers of accumulated bits that a UAV receives, transmits, and buffers are presented. The following observations can be obtained. (1) At any moment, the "received by UAV" curve coincides with the "trx + buffer" curve, indicating that the accumulated received bit number is equal to the sum bits of forwarded and buffered at the UAV. Therefore, information conservation is maintained. (2) At any moment, the accumulated forwarded bit number is smaller than the received bit number, which demonstrates that information causality is maintained. (3) The accumulated buffered bit number first increases and then decreases to zero. This is because initially, the UAV is close to the source node, but far from the destination node, resulting in a better first-hop channel compared to the UAV forwarding channel. Additionally, the first-hop channel capacity is greater than the UAV forwarding channel capacity. The received bits accumulated at the UAV must wait to be forwarded later. As the UAV flies closer to the destination, the UAV forwarding channel becomes stronger than the first-hop channel, leading to a greater forwarding (for outgoing data) channel capacity compared to the first-hop (for incoming data) channel capacity. Therefore, the number of buffered bits decreases.

In Figure 3, the UAV trajectory in the $X - Y$ plane and flying speed in each time interval are presented. In Figure 3 (a), one can see that the optimized trajectory begins from the departure point (ie, (0, 3000)) and ends at the intended destination (ie, (1000, 3000)). Therefore, constraint (19) is satisfied. Additionally, in Figure 3 (b), one can see that $|v_m| \leq 80$ m/s ($\forall m$), implying that constraint (20) is also satisfied.

5.2 | Performance comparisons

To demonstrate the advantages of the proposed FDR UAV scheme, Figure 4 presents EE comparisons between FDR and HDR schemes. Under the HDR scheme [13], the UAV receives data in the first half of each time interval and forwards data in the latter half of each time interval. Generally, the HDR curve is a horizontal line because in the HDR scheme, no SI exists and EE is not affected by the value of k_0. The fluctuation in the "HDR + Optimal Trajectory" curve is caused by the GA's randomness. One can see that the FDR scheme outperforms the HDR scheme when the SI cancelation factor varies between 10^{-6} and 10^{-3}. This is because in scenarios with small SI cancelation factors, the FDR scheme can achieve a higher transmission rate and time efficiency, which is very beneficial in terms of energy saving and EE improvements. However, as the SI cancelation factor increases, the advantages of FDR fade and it becomes even less energy efficient than the HDR scheme. This is because strong SI significantly deteriorates data transmission rates, resulting in a loss of EE. In a practical scenario, the SI cancelation factor is generally less than 10^{-3}.

Additionally, for the FDR scheme, to demonstrate the performance superiority of our trajectory policy, the EE curves for three other benchmark FDR UAV polices are also provided: the "FDR + Straight Trajectory," "FDR + Average Speed," and "FDR + Average Speed + Same Route" policies. Let v_m^*, $v_{x,m}^*$, and $v_{y,m}^*$ represent the optimal flying velocity, flying velocity on the X axis, and flying velocity on the Y axis, respectively, in the m th time interval under the "FDR + Optimal Trajectory" scheme.

TABLE 1 Parameter settings

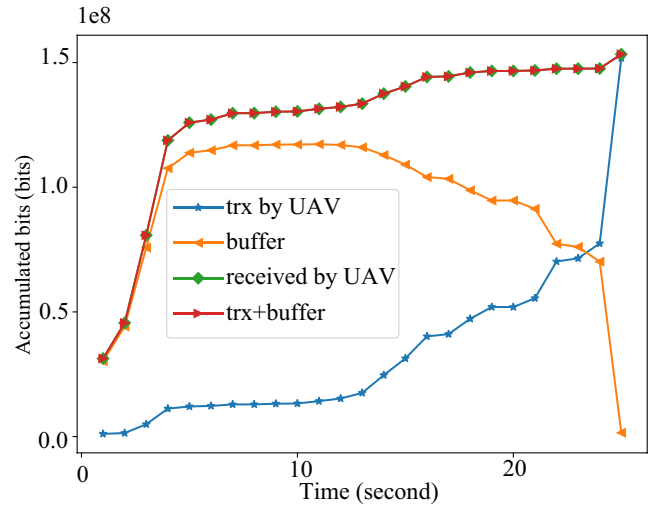| Parameters	Value	Parameters	Value
H	70 m	$V_{\max}$	80 m/s
P_S	0.8 W	P_R	1 W
T	25 s	B	10 MHz
ε	0.012	ρ	1.225
ω	400 dB	$\sigma_1^2 = \sigma_2^2$	10^{-5}
k_h	0.1	W	100
A	0.79	s	0.05
U_{tip}	200	v_0	7.2
η	0.3	R_0	0.5 W
Ω	400	c_1	0.001
c_2	0.001	c_3	1
c_4	5	c_5	9
M	25	(X_0, Y_0)	(0, 3000)
(X_Z, Y_Z)	(1000, 3000)	$a_{1,m} = a_{2,m}$	2
Pr_c	90 %	Pr_v	100 %
$h_{SS} = h_{DD} = h_{RR}$	0.8	$N_{g,\max}$	300
τ	1		

FIGURE 2 Curves of accumulated numbers of bits at UAVs (received, transmitted (or trx), and buffered versus time). The SI cancelation factor $k_0 = 10^{-5}$
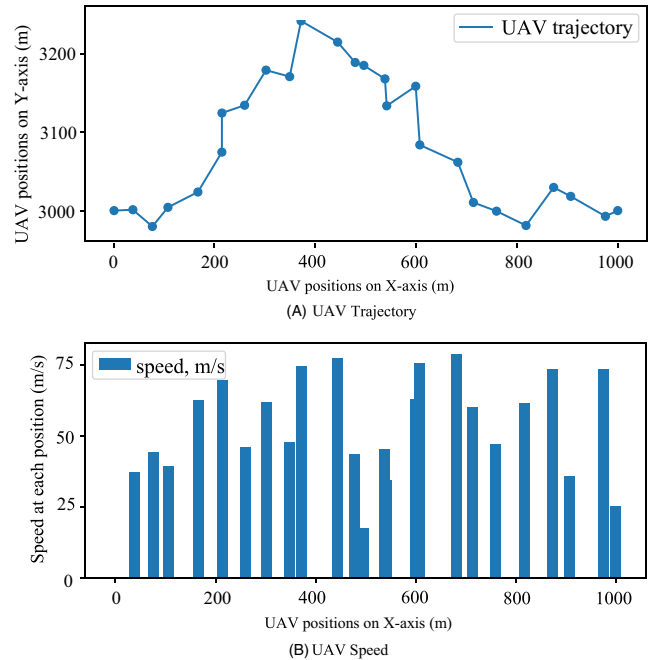

(A) UAV Trajectory

(B) UAV Speed

FIGURE 3 UAV trajectory in the $X - Y$ plane. The SI cancelation factor $k_0 = 10^{-5}$

Under the "FDR + Straight Trajectory" scheme, the UAV flies horizontally and directly along a line from the starting point to the end point within $T = 25$ s. The flight speed of the "FDR + Straight Trajectory" can be calculated as $|v_m'''| = \frac{X_z - X_0}{T} = \frac{1000-0}{25} = 40$ m/s.

Under the "FDR + Average Speed" scheme, the flying velocity in the mth time interval is denoted as $|v_m'| = \sqrt{v_{x,m}'^2 + v_{y,m}'^2}$. We require that (1) $v_m' = \sum_{m=1}^{M} |v_m^*|/M, \forall m$, meaning the flying speed in all time intervals is consistent and takes the
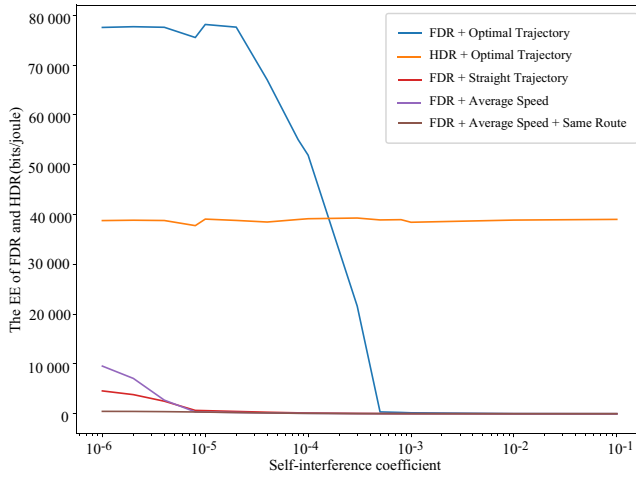
FIGURE 4   EE comparison between FDR and other schemes

FIGURE 5   Convergence behavior of the GA in our FDR UAV system with $k_0 = 10^{-5}$

value of the average speed of the "FDR + Optimal Trajectory." (2) $\frac{v'_{x,m}}{v'_{y,m}} = \frac{v^*_{x,m}}{v^*_{y,m}}$, which guarantees that the bending angle at each knee of the curve is identical to that of the "FDR + Optimal Trajectory." (3) Each time interval must have the same duration (ie, $T/M = 1$s).

Under the "FDR + Average Speed + Same Route" scheme, we require that (1) the flight route is identical to that of the "FDR + Optimal Trajectory" scheme. (2) $v''_m = \sum_{m=1}^{M} |v^*_m|M, \forall m$.

One can clearly see that our "FDR + Optimal Trajectory" scheme outperforms the other FDR benchmark schemes and yields more than five-fold EE gains when $k \leq 10^{-4}$. The reasons for this performance improvement can be summarized as follows. Unlike the other schemes, in the "FDR + Optimal Trajectory" scheme, the flight speeds and directions in all time intervals are jointly maximized. This is because the elitist selection method allows high-quality trajectories to remain for subsequent evolution. As evolution proceeds, high-quality trajectories evolves toward the optimal solution. In contrast, under the "FDR + Average Speed + Same Route" scheme, the flight speed is not optimized, while under the "FDR + Straight Trajectory" and "FDR + Average Speed" schemes, neither the speed nor direction are optimized. Therefore, these schemes perform worse than our "FDR + Optimal Trajectory" scheme.

5.3 | Convergence behavior analysis

Convergence curves are provided in Figure 5. Iteration stops if the predetermined objective function tolerance is satisfied or the maximum iteration number is reached. Specifically, iteration stops if $N_g \leq 300$ or $|\frac{\eta_{EE}(N_g) - \eta_{EE}(N_g-1)}{\eta_{EE}(N_g)}| \leq 10^{-3}$, where 10^{-3} is the predetermined tolerance. Iteration stops at the 80 th generation (ie, 80 iterations). Therefore, the GA converges well for our optimization problem.
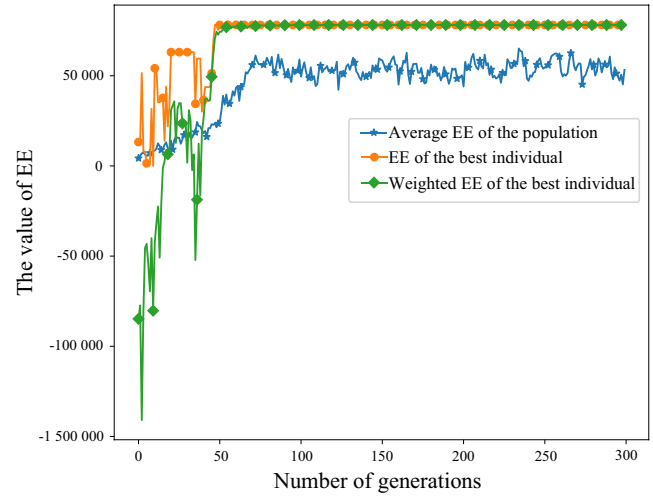
Additionally, it should be noted that the weighted EE is no greater than the EE of the best individual, meaning $\eta^{(w)}_{EE} \leq \eta_{EE}$. As iteration proceeds, the weighted EE and η_{EE} curves overlap, indicating that (20) and (22) are satisfied and no penalties are imposed on the objective function.

6 | CONCLUSIONS

An energy-efficient FDR UAV scheme was investigated in this study. Given an arbitrary radio map, we optimized UAV trajectories under specific constraints for flight behavior and information causality. A GA was designed for our optimization problem, which is applicable to any superposition of small and large fading phenomenon. Numerical results demonstrated that the proposed FDR scheme outperforms HDR schemes and other FDR benchmark schemes. Additionally, the proposed method exhibited desirable convergence behaviors.

ORCID
Nan Qi 🄳 https://orcid.org/0000-0002-0125-370X
Rugui Yao 🄳 https://orcid.org/0000-0003-1396-3802

REFERENCES
1. F. Qi et al., *UAV network and IoT in the sky for future smart cities*, IEEE Netw. **33** (2019), no. 2, 96–101.
2. L. Gupta, R. Jain, and G. Vaszkun, *Survey of important issues in UAV communication networks*, IEEE Commun. Surveys Tuts. **18** (2016), no. 2, 1123–1152.
3. A. Carrascocasado, R. Vergaz, and J. M. Sanchez Pena, *Design and early development of a UAV terminal and a ground station for laser communications*, in Proc. SPIE Int. Soc. Opt. Eng. **8184** (2011), no. 4, 361.

4. J. Tang, L. Fan, and S. Lao, *Collision avoidance for Multi-UAV based on geometric optimization model in 3D airspace*, Arab. J. Sci. Eng. **39** (2014), 8409–8416.

5. B. Li, Z. Fei, and Y. Zhang, *UAV communications for 5G and beyond: Recent advances and future trends*, IEEE Internet Things J. **6** (2019), 2241–2263.

6. C. Cheng et al., *Maximizing throughput of UAV-relaying networks with the load-carry-and-deliver paradigm*, in Proc. IEEE Wirel. Commun. Netw. Conf. (Hong Kong, China), Mar. 2007, pp. 4417–4424. doi: 10.1109/WCNC.2007.805

7. https://spectrum.ieee.org/automaton/consumer-electronics/gadgets/mit-builds-drone-based-rfid-relay-to-track-boxes-in-warehouses

8. http://alpine-robotics.com/projects/future/flying-relay-station/

9. Y. Zeng, R. Zhang, and T. J. Lim, *Throughput maximization for UAV-enabled mobile relaying systems*, IEEE Trans. Commun. **64** (2016), no. 12, 4983–4996.

10. https://dronerush.com/product/parrot-anafi/

11. https://dronerush.com/yuneec-drones-guide-wind-9821/

12. https://dronerush.com/product/dji-mavic-2-zoom/

13. N. Qi et al., *Efficient coded cooperative networks with energy harvesting and transferring*, IEEE Trans. Wirel. Commun. **16** (2017), no. 10, 6335–6349.

14. Q. Wu, Y. Zeng, and R. Zhang, *Joint trajectory and communication design for multi-UAV enabled wireless networks*, IEEE Trans. Wirel. Commun. **17** (2018), no. 3, 2109–2121.

15. W. Wang and H. Yang, *Effect of imperfect spectrum sensing on slotted secondary transmission: Energy efficiency and queuing performance*, IEEE Trans. Cogn. Commun. Netw. **4** (2018), 764–772.

16. Y. Zeng and R. Zhang, *Energy-efficient UAV communication with trajectory optimization*, IEEE Trans. Wirel. Commun. **16** (2017), no. 6, 3747–3760.

17. C. Zhan, Y. Zeng, and R. Zhang, *Energy-efficient data collection in UAV enabled wireless sensor network*, IEEE Wirel. Commun. Lett. **7** (2018), no. 3, 328–331.

18. M. Hua et al., *Outage probability minimization for low-altitude UAV-enabled full-duplex mobile relaying systems*, China Commun. **15** (2018), 9–24.

19. Y. Zeng, R. Zhang, and T. J. Lim, *Wireless communications with unmanned aerial vehicles: Opportunities and challenges*, IEEE Commun. Mag. **54** (2016), 36–42.

20. N. Qi et al., *Energy efficient full-duplex UAV relaying networks under load-carry-and-delivery scheme*, IEEE Access **8** (2020), 74349–74358.

21. M. Alzenad et al., *3-D placement of an unmanned aerial vehicle base station (UAV-BS) for energy-efficient maximal coverage*, IEEE Trans. Wirel. Commun. **6** (2017), 434–437.

22. M. Mozaffari et al., *Optimal transport theory for power-efficient deployment of unmanned aerial vehicles*, in Proc. IEEE Int. Conf. Commun. (ICC), (Kuala Lumpur, Malaysia), May 2016, pp. 1–6, https://doi.org/10.1109/ICC.2016.7510870

23. S. K. Al-Hourani and S. Lardner, *Optimal lap altitude for maximum coverage*, IEEE Wirel. Commun. Lett. **3** (2014), no. 6, 569–572.

24. S. Bhandari and T. Srinivasan, *Path-planning around obstacles for a quadrotor UAV using the RRT algorithm for indoor environments*, in Proc. AIAA Infotech (San Diego, CA, USA), Jan. 2016, https://doi.org/10.2514/6.2016-2196

25. H. Liu et al., *Optimization lighting layout based on gene density improved genetic algorithm for indoor visible light communications*, Optics Commun. **390** (2017), 76–81.

26. G. Shahgholian et al., *A novel approach in automatic control based on the genetic algorithm in statcom for improvement power system transient stability*, in Proc. Int. IEEE Conf. Intell. Syst. (Varna, Bulgaria), Sep. 2008, pp. 4-14–4-19, https://doi.org/10.1109/IS.2008.4670419

27. S. Hashemi et al., *An image contrast enhancement method based on genetic algorithm*, Pattern Recogn. Lett. **31** (2010), no. 13, 1816–1824.

28. P. Devarasetty and S. Reddy, *Genetic algorithm for quality of service based resource allocation in cloud computing*, Evol. Intel. (2019), 1–7.

29. M. Nitti et al., *When social networks meet D2D communications: A survey*, Sensors **19** (2019), no. 2, 396.

30. X. Lin, J. Xia, and Z. Wang, *Probabilistic caching placement in UAV-assisted heterogeneous wireless networks*, Physical Commun. **33** (2019), 54–61.

31. K. Anazawa et al., *Trajectory and data planning for mobile relay to enable efficient internet access after disasters*, in Proc. IEEE Glob. Commun. Conf. (GLOBECOM) (San Diego, CA, USA), Dec. 2015, pp. 1–6, doi: 10.1109/GLOCOM.2015.7417170

32. Y. A. Sambo et al., *Energy minimization UAV trajectory design for delay-tolerant emergency communication*, in Proc. IEEE Int. Conf. Commun. Workshops (ICC Workshops), (Shanghai, China), May 2019, pp. 1–6, doi: 10.1109/ICCW.2019.8757127

33. J. Liu et al., *Age-optimal trajectory planning for UAV-assisted data collection*, in Proc. IEEE Conf. Comput. Commun. Workshops (INFOCOM WKSHPS), (Honolulu, HI, USA), Apr. 2018, pp. 553–558, https://doi.org/10.1109/INFCOMW.2018.8406973

34. S. Bisen and A. V. Babu, *Outage analysis of underlay cognitive NOMA system with cooperative full duplex relaying*, Transac. Emerg. Telecommun. Technol. (2019), e3701.

35. M. Harounabadi, M. Bocksberger, and A. Mitschele-Thiel, *Evolutionary path planning for multiple UAVs in message ferry networks applying genetic algorithm*, in Proc. IEEE Annual Int. Symp. Pers., Indoor Mob. Radio Commun. (PIMRC), (Bologna, Italy), Sept. 2018, pp. 1–7, doi: 10.1109/PIMRC.2018.8580936

36. Y. Zeng, J. Xu, and R. Zhang, *Energy minimization for wireless communication with rotary-wing UAV*, IEEE Trans. Wirel. Commun. **18** (2019), no. 4, 2329–2345.

37. https://dronerush.com/yuneec-drones-guide-wind-9821/

38. https://pan.baidu.com/s/1Wm3k8u_jjgOY3OvP4bW78A

AUTHOR BIOGRAPHIES

Nan Qi received her BS degree and PhD in Communications Engineering from Northwestern Polytechnical University, China, in 2011 and 2017, respectively. From 2013 to 2015, she was a visiting scholar at the Department of Electrical Engineering, KTH Royal Institute of Technology, Sweden. She is currently an assistant professor in the Department of Electronic Engineering, Nanjing University of Aeronautics and Astronautics, China. Her research interests include UAV-assisted communications, mobile edge computing, wireless network protocol design, optimization of wireless communications, network coding, cooperative relaying networks, and wireless energy harvesting and transferring systems.

Wei Wang received his BS degree in Electronic Information Science and Technology from the Anhui University of Finance and Economics, Anhui, China, in 2020. He is currently pursuing his MS degree in Electronic Information at the Nanjing University of Aeronautics and Astronautics.

Diliao Ye received his BE degree in Communication Engineering from Zhejiang University, China, in 2012 and his MS degree in Engineering from the KTH Royal Institute of Technology, Sweden, in 2014. He is currently an engineer ay Telefonaktiebolaget LM Ericsson, Stockholm, Sweden. His research interests include communication theory and 5G/beyond wireless communication systems.

Mei Wang received her BS degree in Electronic Information Science and Technology from the Anhui University of Finance and Economics, Anhui, China, in 2018. She is currently pursuing an MS degree in Signal and Information Processing at the Nanjing University of Aeronautics and Astronautics.

Theodoros A. Tsiftsis received his BS degree in Physics from the Aristotle University of Thessaloniki, Greece, in 1993, MS degree in Digital Systems Engineering from Heriot-Watt University, Edinburgh, UK, in 1995, MS degree in Decision Sciences from the Athens University of Economics and Business in 2000, and PhD in Electrical Engineering from the University of Patras, Greece in 2006. He is currently a professor at the School of Intelligent Systems Science & Engineering of Jinan University, Zhuhai, China, and an Honorary Professor at Shandong Jiaotong University, Jinan, China. His research interests include the broad areas of cognitive radio, communication theory, wireless powered communication systems, optical wireless communication, and ultra-reliable low-latency communication. He has served as a Senior or Associate Editor on the editorial boards of IEEE Transactions on Vehicular Technology, IEEE Communications Letters, IET Communications, and IEICE Transactions on Communications. He is currently an Area Editor for Wireless Communications II of IEEE Transactions on Communications and an associate editor of IEEE Transactions on Mobile Computing. Prof. Tsiftsis has been appointed to a two-year term as an IEEE Vehicular Technology Society Distinguished Lecturer (IEEE VTS DL), Class of 2018.

Rugui Yao received his BS degree, MS degree, and PhD in Telecommunications and Information Systems from the School of Electronics and Information (SEI) of Northwestern Polytechnical University (NPU), Xi'an, China, in 2002, 2005, and 2007, respectively. From 2007 to 2009, he worked as a post-doctoral fellow at NPU. Since 2009, he has worked at the SEI of NPU, Xi'an, China, as a Full Professor. In 2013, he joined the ITP Laboratory at Georgia Tech, Atlanta, USA, as a Visiting Scholar. He has worked in the areas of physical layer security, cognitive radio networks, channel coding, OFDM transmission, and spread-spectrum systems. He is a Senior Member of the IEEE, a Senior Member of the Chinese Institute of Electronics, and a Senior Member of the China Institute of Communications.